

Faculty of Engineering
Faculty of Engineering - Papers

University of Wollongong

Year 2002

A prototype coded aperture detector for
small animal SPECT

S. R. Meikle, *Royal Prince Alfred Hospital, Sydney*

P. Kench, *University of Sydney*

A. G. Weisenberger, *Thomas Jefferson National Accelerator Facility, Virginia, USA*

R. Wojcik, *Thomas Jefferson National Accelerator Facility, Virginia, USA*

M. F. Smith, *Thomas Jefferson National Accelerator Facility, Virginia, USA*

S. Majewski, *Thomas Jefferson National Accelerator Facility, Virginia, USA*

S. Eberl, *Royal Prince Alfred Hospital, Sydney*

R. R. Fulton, *Royal Prince Alfred Hospital, Sydney*

A. Rosenfeld, *University of Wollongong*

M. J. Fullham, *Royal Prince Alfred Hospital, Sydney*

This article was originally published as: Meikle, SR, Kench, P, Weisenberger, AG, Wojcik, R, Smith, MF, Majewski, S, Eberl, S, Fulton, RR, Rosenfeld, AB & Fulham, MJ, A prototype coded aperture detector for small animal SPECT, *IEEE Transactions on Nuclear Science*, October 2002, 49(5)1, 2167-2171. Copyright IEEE 2002.

This paper is posted at Research Online.

<http://ro.uow.edu.au/engpapers/74>

A Prototype Coded Aperture Detector for Small Animal SPECT

Steven R. Meikle, *Senior Member, IEEE*, Peter Kench, Andrew G. Weisenberger, Randy Wojcik, Mark F. Smith, *Member, IEEE*, Stan Majewski, Stefan Eberl, *Member, IEEE*, Roger R. Fulton, *Senior Member, IEEE*, Anatoly B. Rosenfeld, *Senior Member, IEEE*, and Michael J. Fulham

Abstract—In a previous simulation study, we demonstrated the feasibility of using coded apertures together with pixelated detectors for small animal SPECT. In this paper, we further explore the potential of this approach with a prototype detector and simulated multipinhole apertures. We also investigated the effect of multiplexing due to overlapped projections on convergence properties, image signal-to-noise ratio (SNR) and spatial resolution. The detector comprises a 48×44 array of NaI(Tl) crystals, each $1 \text{ mm} \times 1 \text{ mm} \times 5 \text{ mm}$ on a 1.25-mm pitch. The crystal array is directly coupled to a Hamamatsu R3941 8 cm position sensitive photomultiplier tube. Multipinhole apertures were simulated by performing repeated SPECT acquisitions of the same object with a single tungsten pinhole translated to different positions in the aperture plane. Image reconstruction is based on a three-dimensional ray driven projector which is an extension of a method described for single pinhole SPECT with a displaced center of rotation. Image estimates are updated using the maximum likelihood expectation maximization (ML-EM) algorithm. The effect of multiplexing was to slow convergence and reduce the achievable SNR by approximately 15% compared with nonmultiplexed data (but the result may be achieved in a fraction of the time). The reconstructed resolution obtained with a resolution phantom was 1.5-mm full width at half maximum and there was no appreciable difference between the resolution of multiplexed and nonmultiplexed data. These results encourage us to develop a prototype coded aperture system for high sensitivity, high resolution small animal SPECT.

Index Terms—Coded aperture, iterative reconstruction, single photon emission computed tomography (SPECT), small animal imaging.

I. INTRODUCTION

RADIOTRACER imaging of small laboratory animals has emerged as an important tool for studying the molecular origins of human disease and evaluating new forms of therapy. To date, most of this work has been done with dedicated small animal positron emission tomography (PET) systems due to the

high resolution and high sensitivity of this modality. SPECT also has the capability for high resolution imaging, with the added advantages of greater radiotracer availability and longer lived isotopes [1], [2]. However, the main limitation of SPECT is its inferior detection efficiency compared with PET.

Coded apertures were first proposed in nuclear medicine as an alternative to conventional tomography with the advantage of substantially increased detection efficiency [3]–[5]. A multipinhole array, where each pinhole projects an image of the object onto the same detector, is one such example. The increased efficiency is offset because each point in the object is sampled by several points on the detector, i.e., the projection data are multiplexed. As a result of redundancy in the data, the signal to noise advantage over conventional collimation is less than expected when comparing the relative detection efficiencies [6]. In addition, early imaging results were disappointing mainly due to the use of reconstruction techniques which were designed for imaging distant well separated point sources rather than the near field distributed sources encountered in nuclear medicine. However, there is renewed interest in coded apertures because they appear well suited to the geometry of imaging small objects including laboratory animals [7], [8].

We have previously demonstrated the feasibility of using a multipinhole array as an encoding aperture, together with compact high resolution pixelated gamma detectors [9]. In this paper, we further explore the potential of this approach using a prototype detector and simulated multipinhole apertures. We describe our image reconstruction methodology and report the results of studies on the effect of multiplexing on convergence properties, image signal-to-noise ratio (SNR) and spatial resolution. The advantages and limitations of a coded aperture design are discussed in the context of small animal SPECT.

II. METHODS

A. Coded Aperture Detector

The detector comprises a 48×44 array of NaI(Tl) crystals, each $1 \text{ mm} \times 1 \text{ mm} \times 5 \text{ mm}$ on a 1.25-mm pitch. The crystal array is directly coupled to a Hamamatsu R3941 8-cm square position sensitive photomultiplier tube (PS-PMT) whose anode signals are converted to (x, y) position signals by a resistive read-out circuit. The signals are shaped and then sampled by a National Instruments PCI-6110E 4 channel ADC under Kmax

Manuscript received December 12, 2001; revised June 5, 2002.

S. R. Meikle, S. Eberl, R. R. Fulton, and M. J. Fulham are with the Department of Positron Emission Tomography (PET) and Nuclear Medicine, Royal Prince Alfred Hospital, Sydney, NSW 2050 Australia (e-mail: steve@cs.usyd.edu.au).

P. Kench is with the School of Medical Radiation Sciences, University of Sydney, Sydney, NSW 2050, Australia (e-mail: p.kench@cchs.usyd.edu.au).

A. G. Weisenberger, R. Wojcik, M. F. Smith, and S. Majewski are with the Thomas Jefferson National Accelerator Facility, Newport News, VA 23606 USA (e-mail: drew@jlab.org).

A. B. Rosenfeld is with the Medical Physics Research Centre, University of Wollongong, Wollongong, NSW 2522, Australia (e-mail: a.rosenfeld@uow.edu.au).

Digital Object Identifier 10.1109/TNS.2002.803802

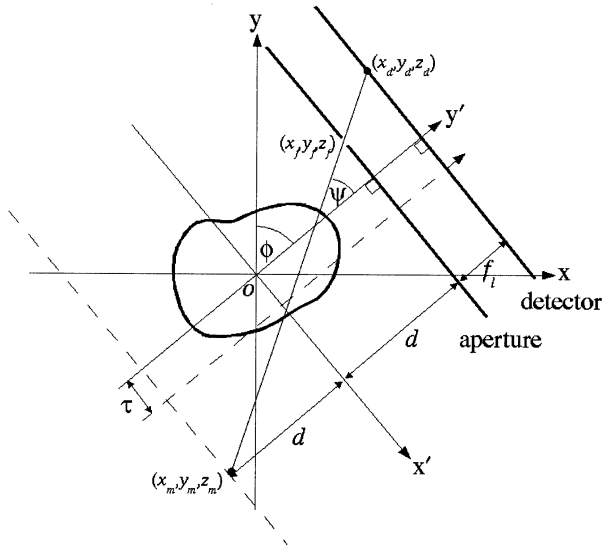


Fig. 1. Imaging geometry for a single pinhole projected onto the x - y plane, with a transaxial component of displacement from the center of rotation θ . The displacement in the axial direction (not shown) is η .

software control.¹ In this paper, individual tungsten pinhole inserts (diameter 0.5 mm) were placed in front of the detector and translated to various positions across the detector field of view to simulate multipinhole arrays.

B. Image Reconstruction

The approach to image reconstruction is similar to that described by Li *et al.* for single pinhole SPECT with a displaced center of rotation [10]. We have extended the method to multiple pinholes, with each pinhole having a unique axial and transaxial displacement from the center of the detector, as well as additional offsets which are common to all pinholes due to mechanical misalignment.

Fig. 1 shows the 3-D imaging geometry projected onto the x - y plane. Let the displacement of a given pinhole from the center of the aperture in the x and z directions be x and z , respectively, and the axial and transaxial components of the rotation misalignment be τ and η . When the detector is rotated through angle ϕ , the coordinates of the pinhole focal point are given by

$$x_f = -d \sin \phi + (x + \tau) \cos \phi \quad (1)$$

$$y_f = d \cos \phi + (x + \tau) \sin \phi \quad (2)$$

$$z_f = z + \eta \quad (3)$$

where d is the perpendicular distance from the aperture to the axis of rotation. We then calculate the coordinates of a mirror point that lies on a line which passes from the detector element through the pinhole focus and intersects a plane parallel to the aperture plane and equidistant from the origin

$$x_m = d \sin \phi - \left(x_d \frac{2d}{f_l} - x - \tau \right) \cos \phi \quad (4)$$

$$y_m = -d \cos \phi - \left(x_d \frac{2d}{f_l} - x - \tau \right) \sin \phi \quad (5)$$

$$z_m = z + \eta - (z_d - z_f) \frac{2d}{f_l} \quad (6)$$

where f_l is the focal length of the pinhole. The coordinates (x_m, y_m, z_m) and (x_f, y_f, z_f) provide the start and end points which can be used with Siddon's ray tracing technique to determine the indices of the voxels that are intersected by the ray and their individual intersection lengths [11]. The element of the transition matrix that describes the probability of a photon emitted from voxel j being detected by detector bin i can then be calculated as

$$p_{ij} = l(j) \cos^4 \psi \exp \left(- \sum_k \mu(j)_k l(j)_k \right) \quad (7)$$

where $l(j)$ is the length of the intersection at voxel j , ψ is the angle from the normal to the detector subtended by the ray, and $\mu(j)_k$ is the attenuation coefficient of the k th voxel intersected by the ray on its way to the detector. The $\cos^4 \psi$ term takes into account the variation in geometric sensitivity and projected volume of the source voxel as a function of ψ , as described by Li *et al.* [10].

The reconstruction is carried out using the familiar update equation of the maximum likelihood expectation maximization (ML-EM) algorithm [12], [13]

$$\lambda_j^{n+1} = \frac{\lambda_j^n}{\sum_i p_{ij}} \sum_i p_{ij} \frac{y_i}{\sum_k p_{ik} \lambda_k^n} \quad (8)$$

where λ^n is the image estimate after n iterations and y are the measured projection data. As with the two-dimensional (2-D) algorithm, the 3-D ML-EM implementation can be regularized using, for example, the one step late approach [14].

C. Convergence and Bias Versus Variance

A source distribution comprising a circular cylinder (2-cm diameter, 2-cm long) centered in a 6 cm \times 6 cm \times 6 cm imaging volume was simulated. The main compartment of the phantom contained uniform activity and there were two smaller cylindrical compartments (7-mm diameter) with 50% less and 50% greater activity, respectively. The source distribution was forward projected through: a) a single pinhole (0.5-mm diameter), and b) an 8-pinhole array (0.5-mm diameter each) using a detector configuration identical to our physical detector with a magnification factor of two at the center of the field of view. In each case, 18 projection views were simulated at 20° increments and Poisson noise was added. During image reconstruction, the mean squared error in voxel values (reconstruction versus actual source distribution) was calculated at each iteration as well as the variance in a background region of interest (ROI) placed in the "warm" part of the phantom.

D. Effect of Multiplexing on SNR

To gain an understanding of the effect of multiplexing on image performance parameters with the 3-D ML-EM algorithm, we performed simulations and phantom experiments where projection data were obtained for individual pinhole inserts at different locations in the aperture plane. This allows the data to be

¹Sparrow Corporation, Starkville, MS 39759-3259

treated as nonmultiplexed (where the projections are kept separate at each view angle) or multiplexed (where the projections are summed at each view angle). This technique is similar to one used by Rowe *et al.* to determine the effective sensitivity of their coded aperture tomograph [6]. The use of nonmultiplexed multipinhole projection data is easily handled by the 3-D ML-EM algorithm by correct specification of the transition matrix.

A uniform cylinder containing 10 MBq of radioactivity was simulated. The cylinder was 2 cm in diameter, 2-cm long and was “imaged” by a detector comprising a 48×44 array of 1 mm crystals on a 1.25-mm pitch. Each simulated SPECT study employed between 1 and 16 pinholes of 0.5-mm diameter and magnification factor 2 at the center of the field of view. At each of 18 projection angles (20° apart), the activity was forward projected and the counts accumulated for 60 s/view, such that each pinhole projected onto a separate “virtual” detector (i.e., up to 16 detectors occupying the same physical location). Poisson noise was added and images were reconstructed using a) non-multiplexed projections (keeping the projections for each pinhole separate) and b) multiplexed projections (where the data corresponding to each view angle were summed). In each case, the reconstruction was stopped after 10 iterations and no regularization or post-reconstruction filtering was applied.

SNR was calculated for each of six central slices, with signal defined as the mean value in a 1-cm diameter circular ROI and noise as the standard deviation in the same ROI. SNR was averaged over the six slices and plotted as a function of detector sensitivity.

E. Effect of Multiplexing on Spatial Resolution

A multiline resolution phantom was used in this experiment. The phantom comprises five line sources of 1-mm diameter and center-to-center spacing of 2, 3, 4, and 5 mm. It was filled with 80 MBq ^{99m}Tc and placed 4.5 cm in front of a 0.5-mm diameter pinhole insert that was placed on a precision X - Y translation stage. The detector was placed 9 cm from the pinhole insert. The phantom was rotated through 18 increments of 20° using a stepper motor under computer control and projection data were acquired for 60 s at each angle. The SPECT acquisition was repeated after the pinhole was translated to a new position in the same plane. In total, four SPECT studies were acquired with the pinhole in different known positions under identical conditions with the acquisition time per angle progressively increased to compensate for loss of sensitivity due to radioactive decay.

As in the simulations, each of the SPECT acquisitions provided a consistent set of projections from a single pinhole with the pinhole having a known displacement from the center of the detector. Summing the four sets of projections provided a simulated multipinhole data set. Thus, we were able to reconstruct images and assess the effect on reconstructed resolution using: a) single pinhole data; b) multipinhole data without multiplexing; and c) multipinhole data with multiplexing. Images were reconstructed using 10 iterations of the 3-D ML-EM algorithm. No regularization or postreconstruction filtering was applied in this case.

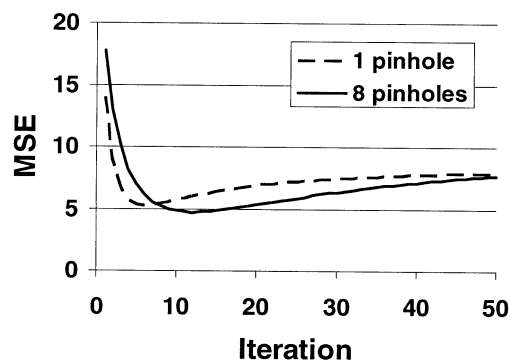


Fig. 2. Convergence of the 3-D ML-EM algorithm for single pinhole and multipinhole projection data.

F. Micro-Derenzo Phantom Study

To assess the performance of the detector and multipinhole reconstruction with a more distributed source, a study was performed using the micro-Derenzo phantom. This phantom has a diameter of 4 cm and comprises 5 sectors of rod sources with diameters ranging from 1 to 2.5 mm and rod separation four times the diameter. The phantom was filled with 164 MBq ^{99m}Tc and positioned on a rotating gantry with the center of rotation 5 cm from the pinhole insert. Because of the restricted field of view of the current detector, it was placed a further 5 cm beyond the pinhole aperture so that there was no magnification at the center of the field of view to ensure the phantom was fully enclosed within the reconstructed field of view. The phantom was rotated through 18 increments of 20° and projection data were acquired for 60 s/angle. The SPECT acquisition was repeated twice with the pinhole translated to a different known position each time using a similar setup to that used for the resolution phantom. For the second and third SPECT studies, the acquisition time per angle was progressively increased to compensate for loss of sensitivity due to radioactive decay.

Images were reconstructed from the single pinhole and multipinhole data using the 3-D ML-EM algorithm. In this experiment, regularization was used in the form of the one step late method [14] and a smoothing prior with only minimal weight applied to the prior ($\beta = 0.05$). Reconstructions were stopped at 100 iterations.

III. RESULTS AND DISCUSSION

A. Convergence and Bias Versus Variance

Convergence of the 3-D ML-EM algorithm is shown in Fig. 2 as mean squared error (mse) versus iteration number. These data indicate that the 3-D ML-EM algorithm is slower to converge for multiple pinhole data than for a single pinhole. We have found that, in general, the greater the degree of overlap of projections, the slower the convergence rate. However, the multipinhole reconstruction achieves less bias at lower variance than in the single pinhole case (Fig. 3).

The slower convergence rate in the case of multipinhole data may be explained by the fact that projections of the source distribution overlap on the detector, resulting in a transition matrix which is less sparse than in the single pinhole case. This points

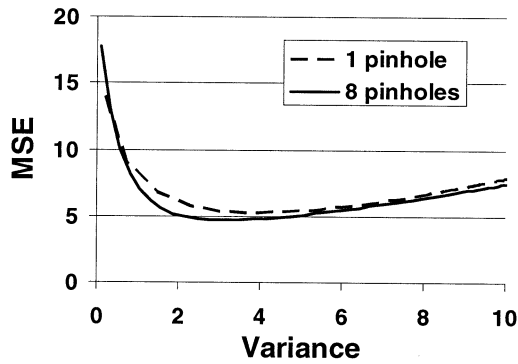


Fig. 3. Bias-variance curve for the 3-D ML-EM algorithm comparing the single pinhole case with the multipinhole case.

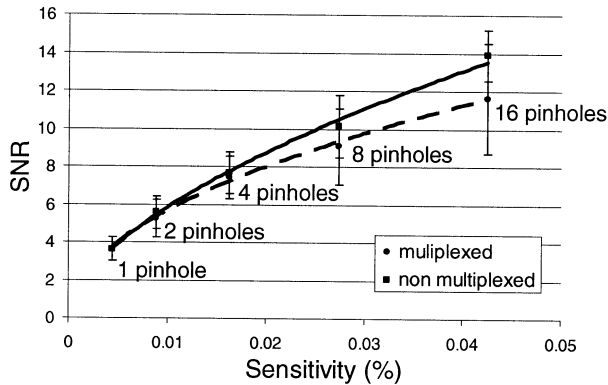


Fig. 4. SNR as a function of detector sensitivity for multiplexed and nonmultiplexed pinhole projection data.

to the need to use more iterations for multiplexed data and suggests that regularization may be required to control the noise which increases with increasing number of iterations.

B. Effect of Multiplexing on SNR

SNR is plotted as a function of detector sensitivity in Fig. 4. The number of pinholes used to achieve a given sensitivity is also indicated on the graph. As expected, SNR increases approximately as the square root of the sensitivity. In the case of multiplexed data, SNR increases with detector sensitivity but the achievable SNR compared with nonmultiplexed data is reduced by approximately 15%. However, it is important to note that the equivalent nonmultiplexed data takes N times longer to acquire than multiplexed data where N is the number of pinholes. This finding is in agreement with that of Rowe *et al.* which they attributed to the fact that each detected photon conveys less information in the multiplexed case than in the nonmultiplexed case due to a degree of ambiguity regarding its origin [6].

C. Effect of Multiplexing on Spatial Resolution

Fig. 5 shows transverse and coronal sections through the reconstructed volumes for the single pinhole and multipinhole cases. There was no appreciable difference in the reconstructed resolution between the three reconstructions as determined by fitting a Gaussian function to one of the line sources in the count density profile and calculating the full width at half maximum (FWHM). Note that, although the FWHM of the profile was similar in all three reconstructions, the first two line sources do

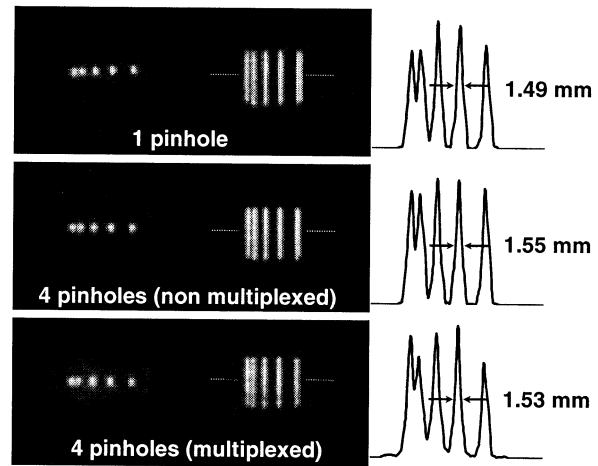


Fig. 5. Transaxial and coronal slices through reconstructed volumes derived from single pinhole and multipinhole projection data. Profiles through coronal slices and corresponding FWHM values are shown at right.

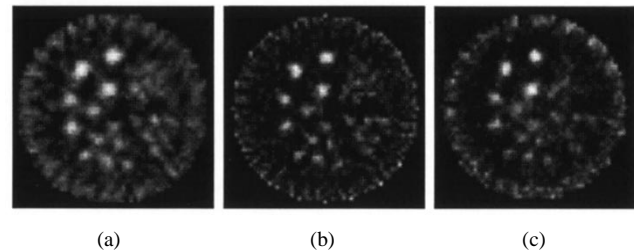


Fig. 6. (a) Transaxial slices through the reconstructed micro-Derenzo phantom using one pinhole. (b) Nonmultiplexed three-pinhole data. (c) Multiplexed three-pinhole data.

not appear to be as well resolved in the multipinhole (multiplexed) case and there appear to be some axial nonuniformities in the coronal section. We believe the slight loss of resolution may be due to the slower convergence when projections are multiplexed (see Figs. 2 and 3) and the source of the axial nonuniformities is currently being investigated.

D. Micro-Derenzo Phantom Study

Transverse slices through the reconstructed volumes are shown in Fig. 6 for the single pinhole and multipinhole cases. The multipinhole reconstructions appear less noisy than the single pinhole reconstruction and the resolution also appears slightly superior. There may be a slight loss of resolution when comparing the multiplexed multipinhole reconstruction with the nonmultiplexed study, although the differences are difficult to discern. Note that the nonmultiplexed data would take three times longer to acquire in practice than the multiplexed data.

The center of rotation offset was measured prior to the three SPECT acquisitions using a line source and a common offset error was applied when reconstructing the single pinhole and multipinhole data. However, it is possible that the mechanical offsets changed slightly during the experiment since, in the case of the multipinhole images, the data are derived from three SPECT acquisitions performed approximately 45 minutes apart. This may account for the apparent differences in reconstructed resolution between the single pinhole and multipinhole studies.

IV. CONCLUSION

Our preliminary data demonstrate the potential of our coded aperture detector and image reconstruction methodology. This approach delivers high spatial resolution which is inherent with pinhole imaging while also providing a substantial increase in sensitivity over conventional single pinhole SPECT. We believe significant improvements in reconstructed spatial resolution will be achieved when larger area detectors are used than the prototype employed in this study, allowing greater magnification of the source distribution.

Further improvements can be anticipated when a more accurate imaging model is employed. The imaging model is relatively simple at present. It assumes perfect pinhole geometry and ignores broadening of the beam due to the finite diameter of pinhole openings and edge effects. Further, we do not model the spatially varying resolution of the detector or depth of interaction effects. It should be noted, however, that the source distributions used in this study comprise mostly high spatial frequency components. Further studies are required to gain a better understanding of the resolution and sensitivity tradeoffs involved when imaging more realistic source distributions. Based on the present work, our main conclusions are as follows.

- 1) The 3-D ML-EM algorithm is suitable for reconstructing multipinhole coded aperture data.
- 2) The effect of multiplexing is to slow convergence and reduce the achievable SNR compared with nonmultiplexed data by approximately 15%.
- 3) There is minimal loss of spatial resolution when reconstructing multiplexed data compared with nonmultiplexed data.
- 4) The accuracy of the imaging model and regularization may be important as the number of pinholes increases (and p becomes less sparse).

In this paper, we used a relatively small number of pinholes to simulate multipinhole acquisition for practical reasons. Therefore, our conclusions apply only to a small number of pinholes and further investigations are required before our conclusions can be generalized to larger pinhole arrays.

REFERENCES

- [1] D. A. Weber and M. Ivanovic, "Ultra-high-resolution imaging of small animals: Implications for preclinical and research studies," *J. Nucl. Cardiol.*, vol. 6, pp. 332–344, 1999.
- [2] S. R. Meikle, S. Eberl, and H. Iida, "Instrumentation and methodology for quantitative pre-clinical imaging studies," *Current Pharm. Design*, vol. 7, pp. 1945–1966, 2001.
- [3] H. H. Barrett, "Fresnel zone plate imaging in nuclear medicine," *J. Nucl. Med.*, vol. 13, pp. 382–385, 1972.
- [4] E. E. Fenimore and T. M. Cannon, "Uniformly redundant arrays: Digital reconstruction methods," *Appl. Opt.*, vol. 20, pp. 1858–1864, 1981.
- [5] G. R. Gindi, J. Arendt, H. H. Barrett, M. Y. Chiu, A. Ervin, C. L. Giles, A. Kujoooy, E. L. Miller, and R. G. Simpson, "Imaging with rotating slit apertures and rotating collimators," *Med. Phys.*, vol. 9, pp. 324–339, 1982.
- [6] R. K. Rowe, J. N. Arrsvold, H. H. Barrett, J.-C. Chen, W. P. Klein, B. A. Moore, I. W. Pang, D. D. Patton, and T. A. White, "A stationary hemispherical SPECT imager for 3-D brain imaging," *J. Nucl. Med.*, vol. 34, pp. 474–480, 1993.
- [7] N. Schramm, A. Wirrwar, F. Sonnenberg, and H. Halling, "Compact high resolution detector for small animal SPECT," *IEEE Trans. Nucl. Sci.*, vol. 47, pp. 1163–1167, 2000.
- [8] D. J. Wagenaar, J. C. Engdahl, V. Simsic, E. G. Hawman, T. Mertelmeier, U. Mahmood, R. Accorsi, and R. C. Lanza, "Use of conventional gamma cameras for small animal imaging," in *Proc. IEEE Nuclear Science Symp. and Medical Imaging Conf.*, vol. 21, Lyon, 2000, pp. 86–90.
- [9] S. R. Meikle, R. R. Fulton, S. Eberl, M. Dahlbom, K.-P. Wong, and M. J. Fulham, "An investigation of coded aperture imaging for small animal SPECT," *IEEE Trans. Nucl. Sci.*, vol. 48, pp. 816–821, 2001.
- [10] J. Li, R. J. Jaszczak, and R. E. Coleman, "Maximum likelihood reconstruction for pinhole SPECT with a displaced center-of-rotation," *IEEE Trans. Med. Imag.*, vol. 14, pp. 407–409, 1995.
- [11] R. L. Siddon, "Fast calculation of the exact radiological path for a three-dimensional CT array," *Med. Phys.*, vol. 12, pp. 252–255, 1985.
- [12] L. A. Shepp and Y. Vardi, "Maximum likelihood reconstruction for emission tomography," *IEEE Trans. Med. Imag.*, vol. MI-1, pp. 113–122, 1982.
- [13] K. Lange and R. Carson, "EM reconstruction algorithms for emission and transmission tomography," *J. Comput. Assist. Tomogr.*, vol. 8, pp. 306–316, 1984.
- [14] P. J. Green, "Bayesian reconstruction from emission tomography data using a modified EM algorithm," *IEEE Trans. Med. Imag.*, vol. 9, pp. 84–93, 1990.